Int. J. Electrochem. Sci., 16 **(2021)** Article ID: 210544, doi: 10.20964/2021.05.58

International Journal of
ELECTROCHEMICAL
SCIENCE
www.electrochemsci.org

Three-dimensional Conducting PEDOT:PSS/MWCNTs Aerogels as Electrochemical Sensing Platform for Sensitive Determination of 2,4-dichlorophenol

Shuxian Chen[1,2], *Qingyun Tian*[1], *Jingkun Xu*[1,3], *Quan Xu*[1], *Xuemin Duan*[1,*], *Xiaoqiang Wang*[2], *Limin Lu*[2,3,*], *Wenchao Dong*[1], *Fan Yang*[1], *Yongfang Yu*[2]

[1] Jiangxi Provincial Key Laboratory of Drug Design and Evaluation, School of Pharmacy, Jiangxi Science and Technology Normal University, Nanchang 330013, PR China
[2] Key Laboratory of Crop Physiology, Ecology and Genetic Breeding, Ministry of Education, Key Laboratory of Chemical Utilization of Plant Resources of Nanchang, College of Science, Jiangxi Agricultural University, Nanchang 330045, PR China
[3] School of Chemistry and Molecular Engineering, Qingdao University of Science and Technology, Qingdao 266042, Shandong, PR China
[*]E-mail: duanxuemin@126.com (X. Duan), lulimin816@hotmail.com (L. Lu).

Received: 3 February 2021 / *Accepted:* 16 March 2021 / *Published:* 31 March 2021

Herein, conducting poly(3,4-ethylenedioxythiophene):poly(styrenesulfonate) (PEDOT:PSS)/MWCNTs aerogels have been employed as sensitive electroanalytical platform for determination of 2,4-dichlorophenol (2,4-DCP). PEDOT:PSS/MWCNTs aerogels were synthesized by the first preparation of PEDOT:PSS hydrogel, followed by injecting MWCNTs suspension into PEDOT:PSS hydrogel and finally freeze drying. The characterization results from scanning electron microscopy (SEM), Raman spectra, and electrochemical measurements indicate that the PEDOT:PSS /MWCNTs aerogels possess hierarchical porous structures, good electrical conductivity, and abundant active sites. The embedding of MWCNTs into PEDOT:PSS aerogels matrix significantly enhances the electrocatalytic performance of the resulting composite aerogels. The PEDOT:PSS/MWCNTs aerogels modified electrode shows excellent electrocatalytic activity to 2,4-DCP oxidation. Accordingly, a low limit of detection of 1.0 nM (S/N= 3) and a wide linear range of 8.0 nM-15.0 μM are achieved. Besides, with satisfactory stability and selectivity, the proposed sensor was successfully applied to detect 2,4-DCP in actual samples.

Keywords: PEDOT:PSS aerogels; MWCNTs; 2,4-dichlorophenol; electrochemical detection

1. INTRODUCTION

Chlorophenols (CPs) are a group of exogenous phenols originated from agricultural and industrial production progresses [1]. Among them, 2,4-dichlorophenol (2,4-DCP) is one of the most

typical CPs, which was widely used in the manufacturing of pharmaceuticals, petrochemicals, dyestuffs, fungicides, pesticides, and herbicides [2-4]. However, 2,4-DCP belongs to persistent organic pollutants (POPs) and has mutagenicity, carcinogenicity, and teratogenicity, giving rise to a great potential threat to human health [3, 5]. Moreover, owing to the increased numbers of chlorine substitutions on the aromatic ring, 2,4-DCP shows a relatively larger bioconcentration factor (log BCF), indicating that 2,4-DCP tends to be accumulated in organisms [6]. Due to the destructive effect on the ecological environment, 2, 4-DCP has been listed as a key contaminant by the U.S. Environmental Protection Agency (EPA) [7, 8].

Conventional analytical methods, such as chromatography and spectrophotometry have been used to detect 2, 4-DCP. However, these techniques involve complicated pre-processing and expensive equipment, which limit the possibility for rapid and economical detection in real samples [9]. On the contrary, electrochemical methods have drawn great attention as a countermeasure due to the rapid, efficient, inexpensive, and on-site detection features. In recent years, several enzyme-based electrochemical biosensors including tyrosinase [10], laccase [11], and horseradish peroxidase [12] have been proposed for highly sensitive and selective detection of 2,4-DCP. However, these enzyme-based sensors always suffer from complicated immobilization steps, unsatisfactory long-term stability and low reproducibility [10, 13]. In this context, nonenzymatic electrochemical sensors based on nanomaterials seem to be a promising technology [2, 14, 15].

High porosity solid nanomaterial aerogels possess the unique characteristics of low density and large internal surface area [16], which are extremely attractive in thermoelectric materials [17, 18], lithium-ion batteries [19], catalysis and sensing applications [20, 21]. Especially, conducting polymer aerogels have been placed great expectations in sensing application due to their characteristic electronic and electrochemical performances. In addition, PEDOT:PSS as a star polymer has been applied to the development of various sensor devices owing to its advantage of prominent environmental stability, approving electrical conductivity, low band-gap, and good mechanical properties [22, 23]. However, to our knowledge, PEDOT:PSS based aerogels have seldom been exploited in electrochemical sensor. The 3D interconnect architectures of PEDOT:PSS aerogels exhibit increased surface areas, enhanced electrical conductivity, and improved heterogeneous electron transfer properties [24, 25]. Furthermore, it is well known that the properties of aerogels are mainly depending on the composite components and their assembly method [26]. It is reported that the composites formed by the coupling of carbon nanomaterials and intrinsically conductive polymers can not only exert the advantages of individual components, but also have synergistic effects [20, 24, 27]. Thus, it is expected that the composite aerogels of PEDOT:PSS/MWCNTs can be an excellent sensing platform for 2,4-DCP detection.

In this study, PEDOT:PSS/MWCNTs aerogels were fabricated by using a facile three-step method. PEDOT:PSS hydrogels were firstly prepared through a hydrothermal process, followed by embedding MWCNTs into PEDOT:PSS hydrogels with the help of injection method. The hydrogel precursors are then freeze-dried to obtain the aerogels of PEDOT:PSS/MWCNTs. Subsequently, the PEDOT:PSS /MWCNTs aerogels modified electrode is utilized as an electrochemical sensor for the electrochemical detection of 2,4-DCP (Scheme 1). The hybridization of PEDOT:PSS aerogels and MWCNTs induce a synergic effect, enhancing the conductivity and giving rise to boosting catalytic

activity. Consequently, the PEDOT:PSS/MWCNTs aerogel electrode high sensing performance towards 2,4-DCP in terms of stability, selectivity, and feasibility. Additionally, the modified electrode is employed for the determination of 2,4-DCP contents in tap water with appropriate recovery.

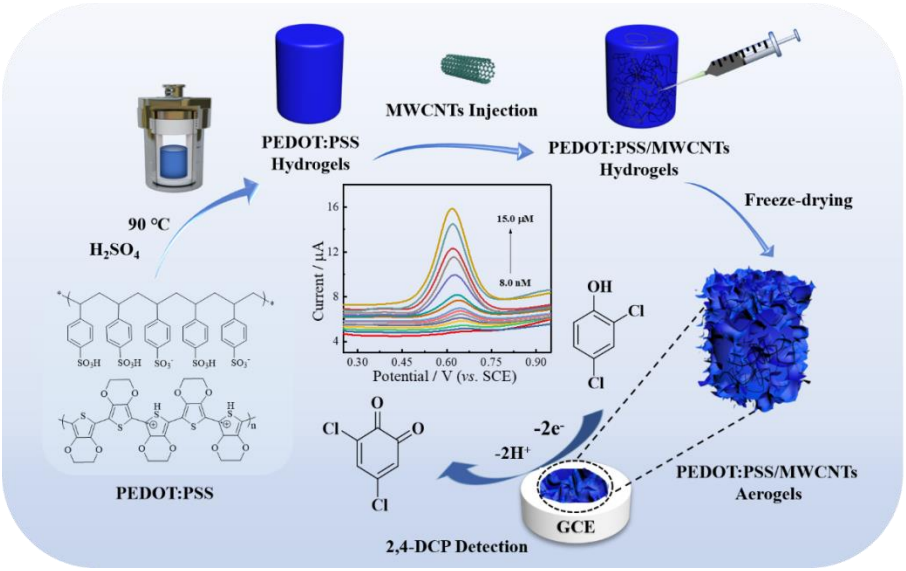

Scheme 1 Synthetic route of PEDOT:PSS/MWCNTs aerogel composite and the sensing strategy for 2,4-DCP.

2. EXPERIMENTAL

2.1. Chemical reagents

Multiwall carbon nanotubes (MWCNTs) were obtained from XF Nano co., Ltd. (Nanjing, China). PEDOT:PSS dispersion (Clevios PH1000) was acquired from Heraeus Precious Metals GmbH & Co. 2,4-dichlorophenol (2,4-DCP), ethanol $NaH_2PO_4 \cdot 2H_2O$ and $Na_2HPO_4 \cdot 12H_2O$ were gained from Sigma-Aldrich. While, the solutions of 2,4-dichlorophenol (2,4-DCP) are prepared by employing ethanol dispersant. The chemical reagents were all analytical reagents.

2.2. Apparatus

Electrochemical workstations with CHI660E model (Shanghai, China) were used for testing electrochemical performance. Electrochemical impedance spectroscopy (EIS) measurements were performed in 5 mM $[Fe(CN)_6]^{3-/4}$ containing 0.1 M KCl with the frequency range from 0.1 to 10000 Hz and the amplitude of 5 mV. LabRAM HR Evolution Raman Spectrometer (Horiba Scientific) was employed to acquire Raman spectra with 785 nm laser source. S-4800 microscope (Hitachi, Japan) was employed to acquire the scanning electron micrograph (SEM) images

2.3. Synthesis of PEDOT:PSS hydrogels

PEDOT:PSS hydrogels were fabricated via a hydrothermal method [28]. 1 mL H_2SO_4 (0.5 M) and 4 mL PEDOT:PSS were mixed and sonicated for 30 minutes. Subsequently, the mixed solution was transferred to Teflon-lined stainless-steel autoclave, which was then reacted at 90 ℃ for 3 h. The acquired gel-like composites were washed with distilled water. The PEDOT:PSS hydrogels were thus obtained for further processing.

2.4. Synthesis of PEDOT:PSS/MWCNTs aerogels

PEDOT:PSS/MWCNTs aerogels were synthesized as follows. The PEDOT:PSS hydrogels were injected with 4 mL MWCNTs suspension. After laying aside for 10 min, the MWCNTs were well dispersed in hydrogel. The PEDOT:PSS/MWCNTs composite hydrogels were then freeze-drying at -60 ℃ for 24 h, and grounded for further application. Pure PEDOT:PSS aerogels were obtained through the similar conditions without the injection of MWCNTs suspension.

2.5. Preparation of modified electrodes

To get 1 mg mL^{-1} PEDOT:PSS/MWCNTs dispersion and PEDOT:PSS dispersion, 10.0 mg PEDOT:PSS/MWCNTs aerogels and 10.0 mg PEDOT:PSS aerogels were ground and ultrasonically dispersed in 10 mL, respectively.

Before modification, 0.5 μm and 0.03 μm alumina slurries were employed to polish the bare GCE. Subsequently, the polished GCE was ultrasonically cleaned with double distilled water and ethanol. Then, 5.0 μL PEDOT:PSS/MWCNTs aerogels dispersion and PEDOT:PSS aerogels dispersion were pipetted onto the GCE surface, respectively, which were dried under an infrared lamp to obtain PEDOT:PSS/MWCNTs aerogels/GCE and PEDOT:PSS aerogels/GCE.

3. RESULT AND DISCUSSION

3.1. Characterization of materials

The surface morphologies of MWCNTs, PEDOT:PSS aerogels, and PEDOT:PSS/MWCNTs aerogels were characterized via SEM. As displayed in Fig. 1A, MWCNTs exhibit long tubular structure. Pure PEDOT:PSS aerogels (Fig. 1B) display a wrinkled lamellar structure. As for PEDOT:PSS/MWCNTs aerogels (Fig. 1C), it can be observed that MWCNTs are dispersed in the lamellar gap of PEDOT:PSS aerogels, which could greatly increase the specific surface area and active-sites of PEDOT:PSS aerogels.

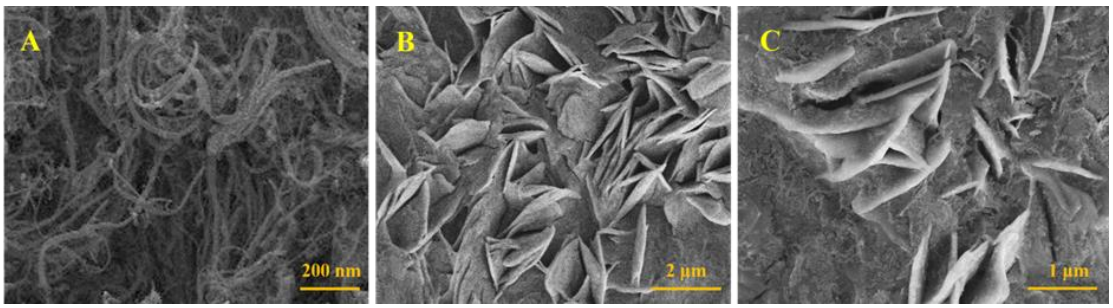

Figure 1. SEM images of MWCNTs (A), PEDOT:PSS aerogels (B), and PEDOT:PSS/MWCNTs aerogels (C)

Raman spectrum was employed to research the structural information of MWCNTs, PEDOT:PSS aerogels, and PEDOT:PSS/MWCNTs aerogels. As displayed in Fig. 2, MWCNTs have the characteristic bands of carbon nanomaterials. The D band at 1345 cm^{-1} means the promiscuous graphitic structure or defect sites of carbon nanotube. While, G band at 1582 cm^{-1} means the vibration of the carbon-carbon double bond [29]. For MWCNTs, the defective sites in the fabrication process of carbon nanotubes are indicated by the D band at 2695 cm^{-1} [30]. For PEDOT:PSS aerogels, the band observed at 1556 cm^{-1} can be allocated to the asymmetrical stretching of C_α=C_β, while the peak at 1443 cm^{-1} is attributed to the symmetrical C_α=C_β stretching [20]. The 1365 cm^{-1} can be assigned to the single C_β=C_β stretching and the 1256 cm^{-1} band represents the C_α=C_α inter-ring stretching [31]. The peaks at 992 cm^{-1} and 576 cm^{-1} are connected with the oxyethylene ring deformation [20]. The peaks at 852 cm^{-1} and 432 cm^{-1} represent the symmetrical C-S-C deformation and SO_2 bending, respectively [32, 33]. As for PEDOT:PSS/MWCNTs aerogels, the Raman spectrum presents both the distinct adsorption peaks of PEDOT:PSS aerogels and MWCNTs, proving the successful preparation of the composite.

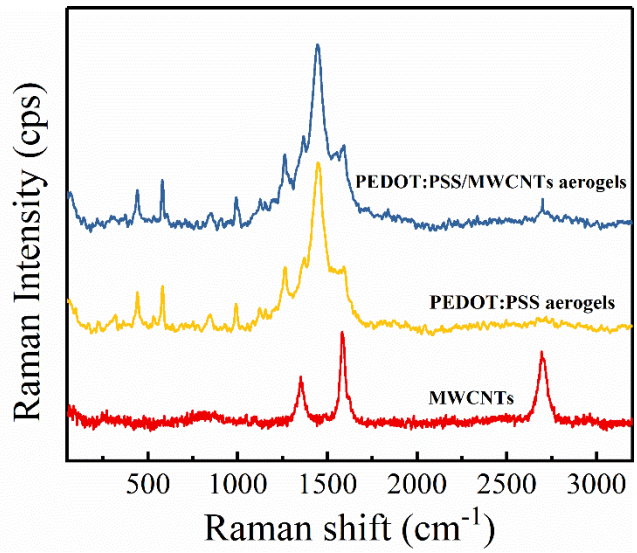

Figure 2. Raman spectrum of MWCNTs, PEDOT:PSS aerogels and PEDOT:PSS/MWCNTs aerogels

3.2. Electrochemical characterization of the modified electrodes

Electron transfer behaviors of the modified electrodes were analyzed by electrochemical impedance spectrometry (EIS) [34, 35]. Generally, the electron transfer-limited process corresponds to the semicircle part at higher frequencies and the semicircle diameter represents the electron transfer resistance (R_{ct}). As can be observed from Fig. 3, compared with bare GCE (a), the R_{ct} values of MWCNTs/GCE (b) and PEDOT:PSS aerogels/GCE (c) decrease, indicating good conductivity of MWCNTs and PEDOT:PSS aerogels. After inserting MWCNTs in PEDOT:PSS aerogels (d), it can be found that the R_{ct} value further reduces, indicating the synergistic effect of PEDOT:PSS aerogels and MWCNTs significantly facilitates the electron-transfer.

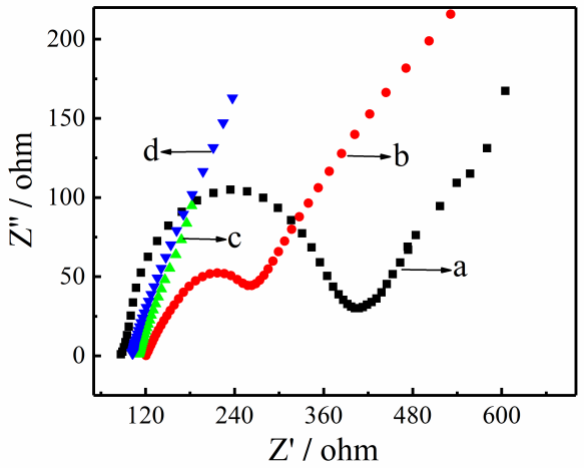

Figure 3. The impedance spectrum of bare GCE (a), MWCNTs/GCE (b), PEDOT:PSS aerogels/GCE (c) and PEDOT:PSS/MWCNTs aerogels/GCE (d) in 5.0 mM $Fe(CN)_6^{3-/4-}$ (1:1) solution containing 0.1 M KCl

3.3. Electrochemical behaviors of 2,4-DCP at different electrodes

The electrocatalytic oxidation behaviors toward 2, 4-DCP were investigated using the differential pulse voltammetry (DPV) method. As displayed in Fig. 4, the electrochemical responses of 10.0 μM 2,4-DCP on bare GCE (a), MWCNTs/GCE (b), PEDOT:PSS aerogels/GCE (c) and PEDOT:PSS/MWCNTs aerogels/GCE (d). As shown, bare GCE (a) displays a small broad peak (a), which is attributed to slow electronic transfer of bare GCE. At MWCNTs/GCE (b), the oxidation peak current increases and the oxidation peak potential decreases, implying the remarkable catalytic activity and conductivity of MWCNTs. As for PEDOT:PSS aerogels/GCE (c), a notably improved peak current is observed, while the oxidation peak potential remains unchanged compared with bare GCE. The phenomenon is owing to the outstanding conductivity and large active surface area of PEDOT:PSS aerogels. Moreover, PEDOT:PSS/MWCNTs aerogels/GCE (d) exhibits a much larger oxidation peak current, resulting from the synergistic effects between PEDOT:PSS aerogels and MWCNTs.

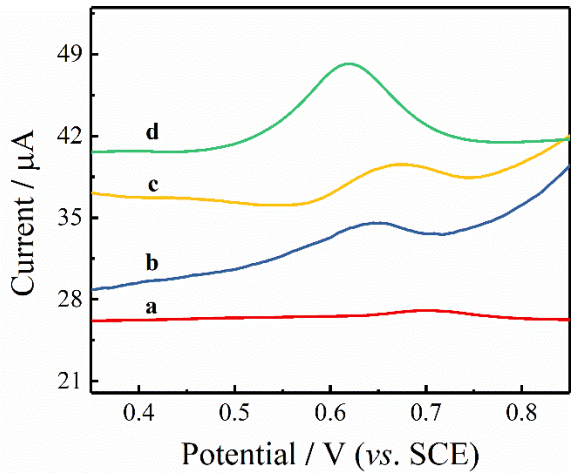

Figure 4. DPVs of bare GCE (a), MWCNTs/GCE (b), PEDOT:PSS aerogels/GCE (c) and PEDOT:PSS/MWCNTs aerogels/GCE (d) in 0.1 M PBS (pH 5.5) with 10.0 μM 2,4-DCP

3.4. Optimization of the experimental parameters

3.4.1. Effect of pH

The effect of pH on the electro-oxidation process toward 1.0 μM 2,4-DCP at PEDOT:PSS/MWCNTs aerogels/GCE was assessed via DPV technology. From Fig. 5A, it can be observed that the oxidation current shows an increasing trend with increasing pH value from 4.5 to 5.5 and then the peak current decreases gradually as the pH range from 5.5 to 7.0. Fig. 5B presents the correlation for the peak oxidation current and the value of pH. The best electrochemical response for 2,4-DCP is obtained at pH 5.5. Thus, pH value is selected as 5.5 in subsequent electrochemical experiments.

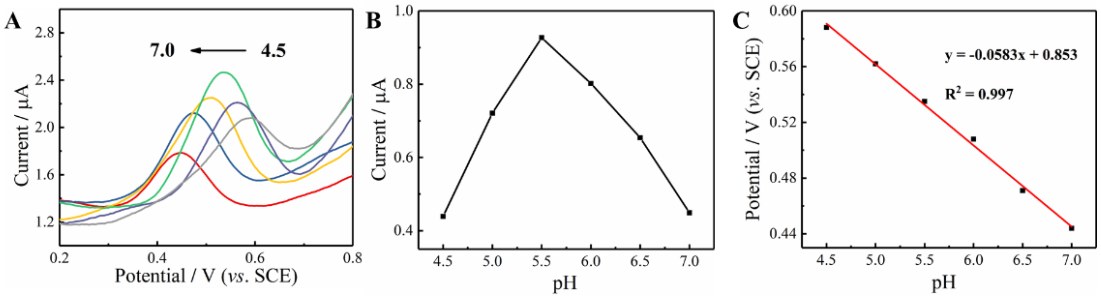

Figure 5. (A) DPVs of PEDOT:PSS/MWCNTs aerogels/GCE in 0.1 M PBS containing 1.0 μM 2,4-DCP with different pH values: 4.5, 5.0, 5.5, 6.0, 6.5, 7.0; (B) Influences of pH on the oxidative peak potential; (C) Influences of pH on the oxidative peak current

Furthermore, it is observed that the oxidation peak potential of 2, 4-DCP shifts to a negative direction from pH 4.5 to pH 7.0, implying that protons were involved in the oxidation reaction. The linear dependence about E_p and pH can be described as $E_p = 0.853 - 0.0583$ pH ($R^2 = 0.997$) (Fig. 5C).

The calculated slope (0.0583 V) is similar to the theoretical value of 0.059 V, demonstrating that the numbers of electrons and protons involved in the electrode reaction of 2, 4-DCP are equivalent [36].

3.4.2. Effect of accumulation time

To improve the amount of 2,4-DCP molecules absorbed at PEDOT:PSS/MWCNTs aerogels/GCE, the effect of the accumulation time on the electrochemical current response of the proposed sensor was assessed by DPVs. As observed from Fig. 6A, the current response of 2,4-DCP increases gradually from 0 to 200 s. However, the oxidation peak response reaches a platform when the accumulation time increases from 200 to 330 s, suggesting that the absorbed amount of 2,4-DCP on PEDOT:PSS/MWCNT$_S$ aerogels/GCE is saturated state [37]. Thus, 200 s is selected as the optimal accumulation time.

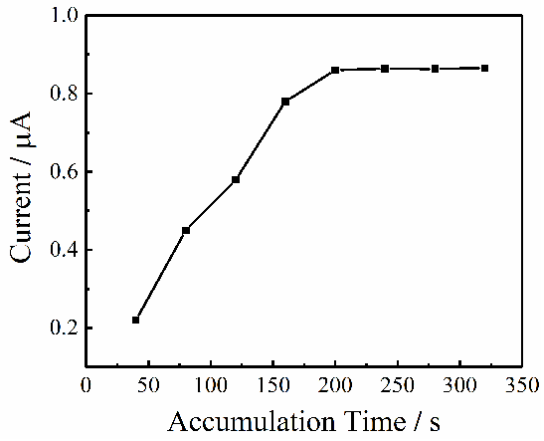

Figure 6. Effect of different accumulation time on peak current of 1.0 μM 2,4-DCP in 0.1 M PBS (pH 5.5) on the PEDOT:PSS/MWCNTs aerogels/GCE

3.4.3. Kinetic characteristic

To understand kinetic characteristic for 2,4-DCP, CVs of 5.0 μM 2,4-DCP were researched at PEDOT:PSS/MWCNTs aerogels/GCE with different scan rates. The anodic peak current (I_{pa}) increases with the increase of the scan rate (v) from 25 to 250 mV s^{-1}. Moreover, there is an outstanding linear function between I_{pa} and v. The fitting equation is formulated as I_p (μA) = 0.0282v + 0.578 (R^2 = 0.995) (Fig. 7B), indicating that the oxidation of 2,4-DCP is an adsorption-controlled process[37].

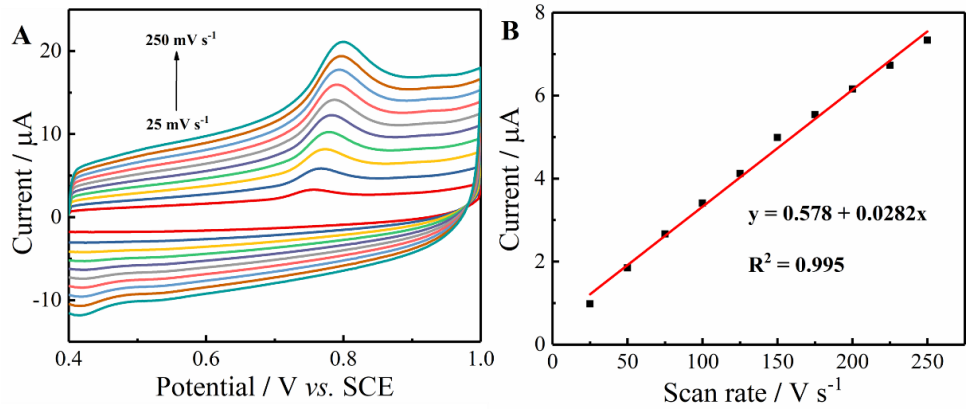

Figure 7. (A) CVs of PEDOT:PSS/MWCNTs aerogels/GCE in present of 5.0 μM 2,4-DCP in 0.1 M PBS (pH 5.5) with different scan rates (25, 50, 75, 100, 125, 150, 175, 200, 225, 250 mV s^{-1}); (B) Linear relationship between the anodic peak currents and the scan rates

3.5. DPV determination of 2,4-DCP at PEDOT:PSS/MWCNTs aerogels/GCE

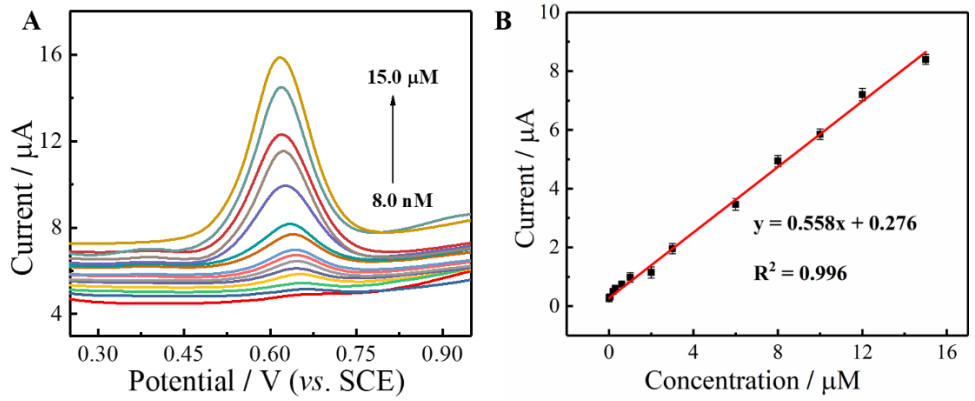

Figure 8. (A) DPVs of 2,4-DCP with different concentrations (0.008, 0.01, 0.05, 0.2, 0.3, 0.6, 1.0, 2.0, 3.0, 6.0, 8.0, 10.0, 12.0, 15.0 μM) using PEDOT:PSS/MWCNTs aerogel/GCE; (B) Linear relationship between peak current and the concentration of 2,4-DCP

Under the optimal experimental parameters, PEDOT:PSS/MWCNTs aerogels /GCE was used to quantitatively analyze 2,4-DCP with different concentration. As observed from Fig. 8A, the anodic peak currents gradually strengthen with the successive addition of 2,4-DCP. In the range from 8.0 nM to 15.0 μM, the linear regression equation between the anodic peak current and 2,4-DCP concentration is I_p = 0.558 C + 0.276 (R^2 = 0.996) (Fig. 8B). The limit of detection (LOD) is calculated to be 1.0 nM (S/N = 3), which is lower than the other reports of 2,4-DCP sensors (Table 1).

Table 1. Comparison of the analytical performance of different 2,4-DCP sensors

Electrodes	Linear range (μM)	LOD (nM)	Ref.
Nafion/MWCNTs[a]	0.1-100.0	37.0	[24]
DGP/GCE[b]	5.0-80.0	250.0	[2]
MoS_2/IL/Au NR/GCE[c]	0.01-50.0	2.6	[8]
$Cu_3(BTC)_2$/CPE	0.04-1.0	9.0	[14]
CS@Ag@GO/GCE[d]	0.05-35.0	7.52	[4]
tyrosinase/MWCNTs/PDDA/GCE	2.0-100.0	660.0	[10]
PEDOT:PSS/MWCNT aerogel/GCE	0.008-15.0	1.0	This work

a: Nafion/Multiwalled carbon nanotubes carbon boron-doped diamond electrode
b: Ternary composite of diamond, graphene, and polyaniline
c: Molybdenum disulfide/Ionic Liquid/Gold Nanorods
d: Graphene oxide nanosheets wrapped core/shell structured carbon sphere@silver
e:Immobilizing tyrosinase on multi-walled carbon nanotubules and polydiallyldimethylammonium chloride

3.6. Repeatability, stability and interference study

To research the repeatability of PEDOT:PSS/MWCNTS aerogels/GCE, a PEDOT:PSS/MWCNTS aerogels/GCE electrode was used for 10 continuous measurements of 5.0 μM 2, 4-DCP. As displayed in Fig. 9A, the relative standard deviation (RSD) is 4.72%, implying a good reproducibility.

Besides, the stability of the PEDOT:PSS/MWCNTs aerogels/GCE was investigated by measuring the change of DPV response toward 5.0 μM 2,4-DCP every two days. The PEDOT:PSS/MWCNTs aerogels/GCE was stored in the air under room temperature. Two weeks later, the DPV current response remains 95.9% of its original response (Fig. 9B), indicating the fabricated electrode exhibits satisfactory long-term stability.

To evaluate the performance on anti-interference of the PEDOT:PSS/MWCNTs aerogels/GCE, the change of DPV current response towards 5.0 μM 2,4-DCP was investigated in the presence of potentially interfering substances. The results are shown in Fig. 10. The signal changes caused by 20-fold concentrations of K^+, Na^+, Ca^{2+}, Cl^-, CO_3^{2-}, NO_3^-, 10-fold biological interferences of ascorbic acid, ferulic acid, and carbolic acid are less than ± 5%. All these results indicate that this sensor owns excellent reliability, reproducibility, and repeatability for the detection of 2,4-DCP.

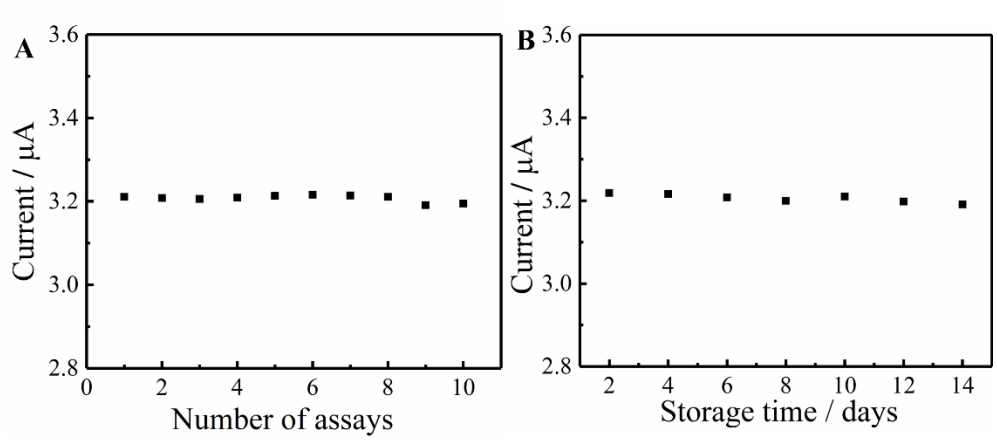

Figure 9. The reproducibility (A) and stability (B) of PEDOT:PSS/MWCNTs aerogels electrode

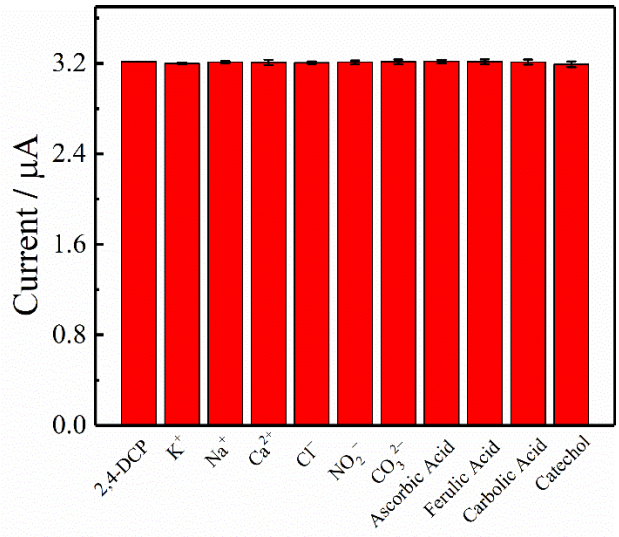

Figure 10. The selectivity of PEDOT:PSS/MWCNTs aerogels electrode

3.7. Determination of 2,4-DCP in real samples

Table 2. Determination of 2,4-DCP in tap water samples using PEDOT:PSS/MWCNTs aerogels electrode (n = 3)

Samples	Added (μM)	Found (μM)	RSD (%)	Recovery (%)
1	0	-	-	-
2	0.5	0.53	2.10	106.0
3	1.00	0.97	4.70	97.0
4	10.00	10.96	1.24	109.6

To validate the application prospect of the PEDOT:PSS/MWCNTs aerogels electrode, it was employed to supervise 2,4-DCP in tap water with standard addition method. The pH value of tap water

sample was buffered close to pH 5.5 with Na_2HPO_4 and NaH_2PO_4. Subsequently, the sample solutions were spiked with a certain concentration of 2,4-DCP standard solution (0.5, 1.0, and 10.0 μM). As displayed in Table 2, the recovery is between 97.0% and 109.6%. Meanwhile, the RSD is between 1.24% and 4.70%. The result means that PEDOT:PSS/MWCNTs aerogel electrode can be applied for the detection of 2, 4-DCP in actual samples.

4. CONCLUSIONS

In this work, by embedding MWCNTs into PEDOT:PSS hydrogels, composite aerogels of PEDOT:PSS/MWCNTs were obtained by freeze-drying of as-prepared composite hydrogel precursors. Subsequently, the PEDOT:PSS/MWCNTs aerogels were applied as electrochemical sensor for the detection of 2,4-DCP. The composite aerogels present the advantages of excellent electrocatalytic activity, good conductivity, high porosity, and large specific surface area, which is helpful to improve the sensing performance. Therefore, PEDOT:PSS/MWCNTs aerogels based electrochemical sensor displays a broad linearity range and low detection limit in 2,4-DCP detection.

ACKNOWLEDGEMENT
We are grateful to the National Natural Science Foundation of China (51762020, 51862014 and 22064010), the Natural Science Foundation of Jiangxi Province (20202ACBL213009), the Open Project of Engineering Center of Jiangxi University for Fine Chemicals (No. KFGJ18018), Collaborative Innovation Center of Jiangxi Typical Trees Cultivation and Utilization (2011), National Students Innovation and Entrepreneurship Training Program (201911318001), and the Jiangxi Provincial Key Laboratory of Drug Design and Evaluation (20171BCD40015) for their financial support of this work.

References

1. Z. N. Garba, W. Zhou, I. Lawan, W. Xiao, M. Zhang, L. Wang, L. Chen and Z. Yuan, *J. Environ. Manage.*, 241 (2019) 59.
2. M. G. Peleyeju, A. O. Idris, E. H. Umukoro, J. O. Babalola and O. A. Arotiba, *ChemElectroChem.*, 4 (2017) 1074.
3. E. O. Igbinosa, E. E. Odjadjare, V. N. Chigor, I. H. Igbinosa, A. O. Emoghene, F. O. Ekhaise, N. O. Igiehon and O. G. Idemudia, *Sci. World J.*, 2013 (2013) 460215.
4. T. Gan, Z. Lv, J. Sun, Z. Shi and Y. Liu, *J. Hazard. Mater*., 302 (2016) 188.
5. M. Pedrero, S. Campuzano and J. M. Pingarron, *J. AOAC Int*., 100 (2017) 950.
6. M. Czaplicka, *Sci Total Environ.*, 322 (2004) 21.
7. R. Sulaiman, M. K. Hadj-Kali, Hasan, S. W. Mulyono S, I. M. AlNashef, *J. Chem. Thermodyn*., 135 (2019) 97.
8. H. Huang, M. Wang, Y. Wang, X. Li, Z. Niu, X. Wang and J. Song, *Microchim. Acta*, 185 (2018) 292.
9. W. Du, F. Zhao and B. Zeng, *J. Chromatogr. A*, 1216 (2009) 3751.
10. L. Kong, S. Huang, Z. Yue, B. Peng, M. Li and J. Zhang, *Microchim. Acta*, 165 (2008) 203.
11. J. Liu, J. Niu, L. Yin and F. Jiang, *Analyst,* 136 (2011) 4802.
12. Y. Zhang, J. Zhang, H. Wu, S. Guo and J. Zhang, *J. Electroanal. Chem*., 681 (2012) 49.

13. F. Karim, A. N. M. Fakhruddin, *Rev. Environ. Sci. Bio/Technol*., 11 (2012) 261.
14. S. Dong, G. Suo, N. Li, Z. Chen, L. Peng, Y. Fu, Q. Yang and T. Huang, *Sensors Actuators B Chem.*, 222 (2016) 972.
15. J. Zhang, J. Lei, H. Ju and C. Wang, *Anal. Chim. Acta*, 786 (2013) 16.
16. N. H. s. a. U. Schubert, *Angew. Chem. Int. Ed*., 37 (1998) 22.
17. M. P. Gordon, E. W. Zaia, P. Zhou, B. Russ, N. E. Coates, A. Sahu and J. J. Urban, *J. Appl. Polym. Sci.,* 134 (2017) 44070.
18. X. Sun, Y. Wei, J. Li, J. Zhao, L. Zhao and Q. Li, *Sci. China Mater*., 60 (2017) 159.
19. Y. Wang, Y. Jin, C. Zhao, E. Pan and M. Jia, *J. Colloid Interface Sci*., 532 (2018) 352.
20. Y. Ma, N. Wei, Q. Wang, C. Wu, W. Zeng, Y. Gao, C. Xu, L. Huang and J. Zhao, *Adv. Electron. Mater.,* 5 (2019) 1900637.
21. Y. Xie, X. Tu, X. Ma, M. Xiao, G. Liu, F. Qu, R. Dai, L. Lu and W. Wang, *Electrochim. Acta*, 311 (2019) 114.
22. Q. Tian, J. Xu, Q. Xu, X. Duan, F. Jiang, L. Lu, H. Jia, Y. Jia, Y. Li and Y. Yu, *Microchim. Acta*, 186 (2019) 772.
23. Q. Tian, J. Xu, Y. Zuo, Y. Li, J. Zhang, Y. Zhou, X. Duan, L. Lu, H. Jia, Q. Xu and Y. Yu, *J. Electroanal. Chem.,* 837 (2019) 1.
24. X. Zhang, J. Liu, B. Xu, Y. Su and Y. Luo, *Carbon*, 49 (2011) 1884.
25. X. Zhao, W. Wang, Z. Wang, J. Wang, T. Huang, J. Dong and Q. Zhang, *Chem. Eng. J.*, 395 (2020) 125115.
26. A. R. Spencer, A. Primbetova, A. N. Koppes, R. A. Koppes, H. Fenniri and N. Annabi, *ACS Biomater. Sci. Eng*., 4 (2018) 1558.
27. J. Zhou and Y. L. Hsieh, *ACS Appl. Mater. Interfaces*, 10 (2018) 27902.
28. B. Yao, H. Wang, Q. Zhou, M. Wu, M. Zhang, C. Li and G. Shi, *Adv. Mater*., 29 (2017) 1700974.
29. J. H. Lehman, M. Terrones, E. Mansfield, K. E. Hurst and V. Meunier, *Carbon*, 49 (2011) 2581.
30. K. Koteshwara Reddy, M. Satyanarayana, K. Yugender Goud, K. Vengatajalabathy Gobi and H. Kim, *Mater. Sci. Eng*. C., 79 (2017) 93.
31. T. Kim, S. Park, J. Seo, C. W. Lee and J.M. Kim, *Org. Electron*., 74 (2019) 77.
32. F. Jiang, J. Xiong, W. Zhou, C. Liu, L. Wang, F. Zhao, H. Liu and J. Xu, *J. Mater. Chem*. A, 4 (2016) 5265.
33. A. A. F. Antje Schaarschmidt, A. Aby, and A. S. Helmy, *J. Phys. Chem*. B, 113 (2009) 9352.
34. F. Gao, X.Tu, X. Ma, Y. Xie, J. Zou, X. Huang, F. Qu, Y.Yu, L.Lu, *Talanta*, 215 (2020) 120891.
35. O. Zhang, Y. Wen, J.Xu, L. Lu, X.Duan, H. Yu, *Synth. Met.,* 164 (2013) 47.
36. Y. Liang, L.Yu, R.Yang, X. Li, L. Qu, J. Li, *Sens. Actuators* B Chem., 240 (2017) 1330.
37. J. Li, D. Miao, R. Yang, L. Qu, P. D. B. Harrington, *Electrochim. Acta*, 125 (2014) 1.